applied sciences

MDPI

Article

Organic Petrologic Characterization and Paleoenvironmental Analysis of Permian Shale in Northeast Sichuan Province, China

Chao Jiang [1] and Xiaomin Xie [2,3,*]

[1] School of Earth Sciences, Yangtze University, Wuhan 430100, China; 2021710385@yangtzeu.edu.cn
[2] School of Resources and Environment, Yangtze University, Wuhan 430100, China
[3] Key Laboratory of Oil and Gas Resources and Exploration Technology, Ministry of Education, Wuhan 430100, China
* Correspondence: xiaominxie2019@sina.com

Abstract: The Permian shale in Northeast Sichuan is an important shale oil and gas resource potential area, and the study of its organic matter characteristics and paleoenvironmental analysis is of great significance for revealing the shale oil and gas formation mechanism and resource evaluation. In this study, the organic matter of Permian shales in northeast Sichuan was carefully studied based on various analytical tools, such as petrology, laser Raman, microscopy, and principal trace elements, and the paleoenvironmental parameters of the shales were comprehensively analysed. A detailed study of the organic matter characteristics of Permian shales in northeast Sichuan reveals important features such as organic matter fractions, structural characteristics, maturity and sources. The results show that the organic matter of the shale consists mainly of solid bitumen, putrescine group, specular group and multicellular planktonic algae. Petrological observations and laser Raman analyses indicate a high maturity of the organic matter and a high content of organic carbon (TOC), showing good hydrocarbon potential. In this study, we reconstructed the palaeoenvironmental parameters and inferred the palaeoenvironmental evolution through palaeoenvironmental analyses of Permian shales in northeast Sichuan. The results of the comprehensive multi-indicator study show that the type of palaeoenvironment at the time of shale deposition was mainly an anoxic-reducing environment, and the depositional conditions were favourable to the enrichment and preservation of organic matter. In summary, the organic matter characteristics and paleoenvironmental analyses of the Permian shales in Northeast Sichuan provide important geological background information for an in-depth understanding of the formation mechanism, exploration potential and development prospect of shale hydrocarbons in this area. The results of this study can provide a scientific basis for the evaluation and development of shale oil and gas resources in this area, which is of great significance to geologists and the energy industry.

Keywords: Northeast Sichuan; Permian shale; organic matter characteristics; palaeoenvironmental analyses; resource evaluation; development prospects

Citation: Jiang, C.; Xie, X. Organic Petrologic Characterization and Paleoenvironmental Analysis of Permian Shale in Northeast Sichuan Province, China. *Appl. Sci.* **2024**, *14*, 2792. https://doi.org/10.3390/app14072792

Academic Editor: Nikolaos Koukouzas

Received: 18 January 2024
Revised: 7 March 2024
Accepted: 22 March 2024
Published: 27 March 2024

1. Introduction

Shale gas is a self-generating and self-storing natural gas system [1,2], which is one of the most important petroleum resources of recent years. The Sichuan Basin is a key target for shale gas exploration in China [3–8]. Numerous studies have significantly revealed the tectonic, petrological, geochemical and petrophysical characteristics of this gas shale section [9–16]. Among the numerous findings, it is a well-known fact that total organic carbon (TOC) in shale gas systems is positively correlated with shale gas content [17–19]. Wu et al. obtained a moderately positive correlation (R^2 = 0.667) between shale gas content and TOC content in the Fuling field in the Sichuan Basin [19].

The exploration and development of shale gas in China has made major breakthroughs in recent years. The shale gas of the Wufeng-Longmaxi Formation in Changning and the

Zhaotong, Weiyuan and Jiaoshiba blocks in Sichuan Basin has been commercially produced, and the daily shale gas production of the Jiaoshiba block reached 3.1×10^6 m^3 in May 2014 [20,21]. Nevertheless, no other blocks in the Sichuan Basin have obtained commercial gas flow except the four blocks mentioned above. Comparison shows that the four blocks are all in regions with a simple structure [22–24], while the exploration and development of shale gas in complicated structural areas has not yet realized a breakthrough.

With the rapid development of China's economy, the demand for oil and gas resources is increasing. Therefore, in recent years, China has put forward strategic requirements for vigorous development of gas (especially shale gas) and improvement of domestic oil/gas supply capacity. In recent years, China's shale gas industry has been developing rapidly, and major breakthroughs have been made in the exploration of two sets of organic-rich marine shale widely developed in the Lower Palaeozoic in the south. Land-phase shale oil and gas, on the other hand, is another important new area for shale oil and gas exploration and development in the Sichuan Basin. The Northeast Sichuan area has been proven to have developed a number of stratigraphic formations with marine-land superposition, and industrial gas flow has been obtained in a number of stratigraphic systems, which are key areas for natural gas exploration in the Sichuan Basin [25–27]. The development of high-quality hydrocarbon source rocks in the marine phase is the necessary material basis for the formation of large oil and gas fields. With regard to the geochemical characteristics and developmental environments of several marine hydrocarbon source rocks in Northeast Sichuan, a lot of research work has been carried out in the past, mainly focusing on the Cambrian and Permian hydrocarbon source rocks. In recent years, the hydrocarbon source rocks of the Upper Permian Dalong Formation, Wujiaping Formation, and Maokou Formation have received more and more attention [28–30].

Organic matter serves as the main carrier of shale hydrocarbons, and the hydrocarbon potential of hydrocarbon source rocks is in turn related to organic matter abundance, organic matter type and organic matter maturity. A large number of exploration studies have shown that the marine shales in the Sichuan Basin have a large hydrocarbon potential, so the organic matter characteristics of the Permian shales in Northeast Sichuan studied in this paper are of great significance. This shale has high organic matter abundance; the organic matter type is mainly I-II_2, and the organic matter is in the high-overmature stage, which is fully consistent with the characteristics of high-quality hydrocarbon source rock. In order to more objectively and accurately identify the developmental characteristics of different microscopic components, taking the Permian shale in northeast Sichuan as the research object, the author used the combination of optical microscopy and laser Raman to observe the developmental characteristics of different microcomponents in situ, so as to provide a theoretical basis for the effective exploration and development of Permian marine shale gas in the Sichuan Basin in the later period [31–33]. Overall, the current research status of organic petrological characteristics and palaeoenvironmental analyses of the Permian shales in northeast Sichuan shows that the organic matter type and abundance are high, the maturity is relatively mature, microbial action may have an influence on shale evolution, and the depositional environment is mainly lake and wetland deposition. Both domestic and international studies provide important theoretical and technical support for the exploration and development of shale gas resources in northeast Sichuan [34,35].

2. Geological Settings

The Sichuan Basin covers an area of about 190,000 km^2 and is a large craton basin, containing up to 6–12 km of Aurignacian to Quaternary sediments. The basin basement is often referred to as the Yangzi quasi-platform, formed during the Jinning (850 Ma) and Chengjiang (700 Ma) orogenic movements; it then crystallised and deteriorated before the Late Aurignacian [36–41]. The tectonic evolution of the Sichuan Basin has undergone a transition from a relatively stable to a relatively unstable phase of the craton. Regional uplift in the Early Palaeozoic (to Early Permian) resulted in large-scale uplift and depression tectonics. Beginning in the Devonian, tensional faulting occurred along the margins of the craton in the context of the Caledonian uplift and depression and gradually extended into the terrane [42–46]. Basal eruptions occurred along certain rift depression zones through the Middle Carboniferous, and the pull-apart movement culminated in the Permian with large-scale basaltic eruptions over the Upper Yankton craton. In the Early and Middle Triassic, due to the extrusion of the Tethys and the Pacific Ocean, the margins of the craton were uplifted, forming algal and oolitic beaches, which blocked the seawater and made the central part of the basin a salt-bearing basin. At the end of the Triassic, several phases of the Indo-Chinese orogeny were superimposed, forming large folds, and Sichuan began the stage of terrestrial sedimentary development [47–50]. From the Jurassic to the Early Cretaceous, the western margin of the basin was uplifted several times, and each uplift was accompanied by a strong depression in the mountain front. This resulted in a continental basin configuration characterised by a depression around an uplifted centre. The Early Cretaceous to Late Cretaceous uplifted the eastern part of the Kawarthas, and no sediments were deposited thereafter. In contrast, western Sichuan deposited continuous sediments during the Cretaceous and Neoproterozoic, and the lake basin gradually contracted to the west. The Himalayan orogeny led to three phases of intense folding in western Sichuan. This orogenic movement corresponds to the Tethys closure period, and the effects of subduction of the Pacific Plate are evident in eastern Sichuan. Counterclockwise coupling is the basic stress that forms the diamond-shaped tectonic basin in Sichuan. The study area is located in the northeastern part of the Sichuan Basin as shown in Figure 1 below [51–56].

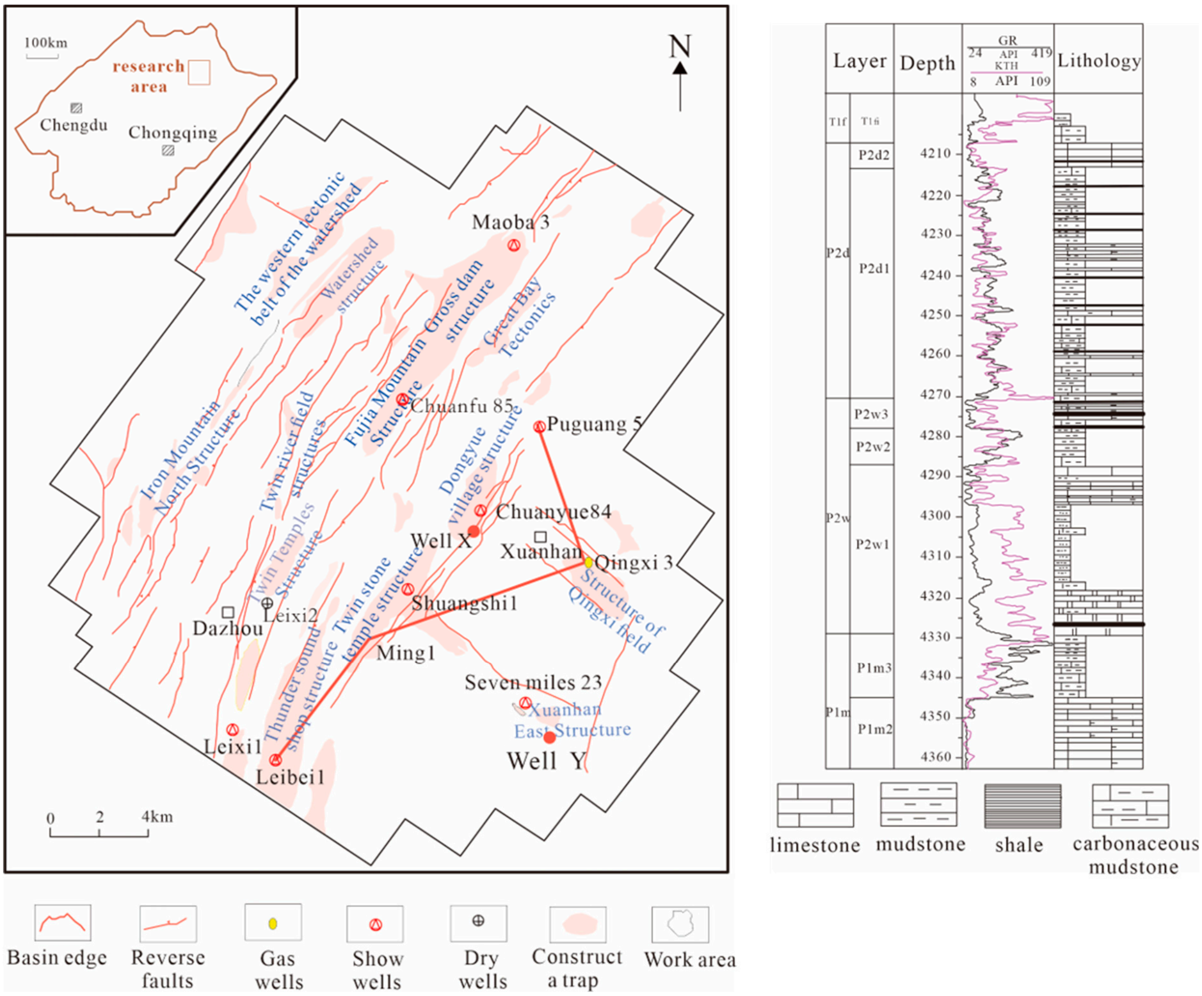

Figure 1. Tectonic trap and well location distribution map in northeast Sichuan. The graph on the right is a bar graph of well X.

3. Materials and Methods

3.1. Shale Samples

A total of 40 shale core samples were taken from two wells, X and Y, in the northeastern Sichuan Basin. The main formations in well X are the Dalong Formation, Wujiaping Formation and Maokou Formation; the main layers in well Y are the Wujiaping Formation and Maokou Formation. Sampling depth of well X: 4213.35–4335.0 m; sampling depth of well Y: 3295.6–3355.47 m. Of these samples, all 15 from the Dallon Formation were taken from the X well; 15 in the Wujiaping Formation, including 8 in X wells and 7 in Y wells; 10 from the Maokou Formation including 3 from well X and 7 from well Y; samples totalled 40. The list of samples is given in Tables 1 and 2 below.

Table 1. List of samples from Permian X wells in northeastern Sichuan.

Sample Number	Wells	Sampling Depth/m	Stratum	TOC (%)
X-1	Well X	4213.35	Dalong Formation	1.23
X-2		4216.25		1.65
X-3		4224.91		2.60
X-4		4229.1		1.63
X-5		4234.69		2.49
X-6		4243.1		2.87
X-7		4244.71		5.03
X-8		4247.13		8.00
X-9		4250		0.80
X-10		4253.69		5.07
X-11		4261.76		11.20
X-12		4263.09		6.10
X-13		4266.63		7.75
X-14		4268.47		6.55
X-15		4270.39		0.83
X-16		4278.59	Wujiaping Formation	7.63
X-17		4280.78		3.92
X-18		4290.4		5.98
X-19		4296.87		0.57
X-20		4297.28		10.90
X-21		4301.53		3.23
X-22		4310.39		4.69
X-23		4314.24		4.41
X-24		4330.48	Maokou Formation	17.10
X-25		4331.9		3.60
X-26		4333.75		5.57

Table 2. List of samples from Permian Y wells in northeastern Sichuan.

Sample Number	Wells	Sampling Depth/m	Stratum	TOC (%)
Y-1	Well Y	3295.6	Wujiaping Formation	12.27
Y-2		3301.3		8.76
Y-3		3304		16.98
Y-4		3307.9		8.18
Y-5		3308.7		4.78
Y-6		3323.38		6.80
Y-7		3324.38		14.70
Y-8		3333.54	Maokou Formation	2.50
Y-9		3339.04		1.73
Y-10		3340.54		1.86
Y-11		3345.07		16.70
Y-12		3350.57		18.20
Y-13		3353.07		16.95
Y-14		3355.47		13.31

3.2. Total Organic Carbon

After initial screening of sample hand specimens for higher clay content, the samples were crushed to 200 mesh; dilute hydrochloric acid was added and the samples were heated in an ultrapure water bath for 2 h, washed and dried. Total organic carbon (TOC%) and total sulphur (S%) results were obtained for the treated samples using the CS230PCHC carbon and sulphur results. The experiment is based on GB/T 19145-2022 [57] "Determination of Total Organic Carbon in Sedimentary Rocks", for evaluating organic matter abundance and establishing the relationship between elemental carbon and sulphur.

3.3. Organic Petrology

In this study, the characteristics of hydrocarbon source rocks in different layers in terms of hydrocarbon generating materials and depositional environments were investigated by combining organic petrology and geochemical methods. Using a sample light film using a MF43 micro fluorescence spectrometer based on SYT 5124-2012 [58] "Method for Determination of Specular Reflectance in Sedimentary Rocks", the specular reflectance value (%Ro) was measured by using the difference between the specular body in grey scale and the standard sample. Optical thin sections for identification of minerals and organic matter were studied using transmittance, polarisation, reflectance and fluorescence in a microfluorescence spectrometer model MF43. The identification standard is SY/T 6414-2014 [59] "Identification and Statistical Methods of Microscopic Composition of Whole Rock Light Flakes".

3.4. Primary and Trace Elements

Trace element analysis was performed using inductively coupled plasma mass spectrometry (ICP-MS). About 50 mg of each sample ground greater than 200 mesh was treated with 1.5 mL of HNO_3, 1.5 mL of HF and 0.01 mL of $HClO_4$ in an open-top Teflon beaker on a hot plate at about 140 °C. After evaporation to wet salt conditions, a mixture of 3 mL of HNO_3 and HF (*v*:*v*, 1:1) was added to the residue and again heated at about 195 °C for more than 48 h. After complete evaporation of the acid, the residue was dissolved in 3 mL of HNO3 and heated to wet salt conditions. Then, 3 mL of HNO_3 was added and the residue was heated at 150 °C for 24 h to ensure complete evaporation of the acid. After cooling, 2 mL of 5 MHCl was added to the resulting dried residue and the sample was extracted at 60 °C for 1 h. Finally, the material was cooled again and 8 mL of H_2O was added; the solution was placed in a vortex mixer, decanted into a new test tube and diluted with 2% HNO_3 for analysis. To check the analytical accuracy and precision of the master trace element data, it was used as the certified reference sample. Each sample was analysed three times and the final average result was used. The analytical precision for the primary trace elements was estimated at 5 percent.

3.5. Laser Raman

Raman spectroscopy is based on the Raman scattering effect. By analysing the parameters of the G and D peaks of a sample, information about molecular vibrations and rotations can be obtained. Raman spectroscopy experiments on shale samples were performed using a Renishaw inVia Raman microscope. The argon ion laser was excited with a 532 nm laser, which was focused on the surface of the microcomponent with a 50× magnifying objective, producing a spot size of 2 μm. The laser power was set to 1 mW and the grating was set to 1800 lines/mm. Spectra were obtained in the range of 500–2500 cm^{-1}. Prior to testing, wave number calibration was performed using a silicon wafer, and Raman spectra were collected for each sample. Curve-fitting and baseline-corrected reflectance and G- and D-band parameters were determined by testing carbonaceous material, coal, shale, oil matrices, specular plasmas, solid asphalt, and animal detritus, including spectral band position, spectral band separation, spectral band intensity ratios, and half-peak widths (FWHM).

4. Experimental Results

4.1. Organic Petrological Characteristics

The results of organic matter microcomposition show that the Permian hydrocarbon source rocks in Northeast Sichuan differ greatly in different layers of the Dalong, Wujiaping and Maokou Formations, reflecting the different sources of organic matter. The specular groups in the hydrocarbon source rocks are less developed and are mainly dominated by the corrosive mud groups, with a very small amount of chitinous and inert groups. Based on the casein carbon isotope study, the previous researchers concluded that the organic matter type of Dalong Formation shale is dominated by II_2-III type, i.e., the main body is the humic type, which is very different from the I-II_2 type of organic matter revealed by the study of Ting Jianghui. The difference is likely to be due to the fact that casein carbon isotope is affected by the combination of various factors, such as the hydrocarbon parent material and the degree of thermal evolution of the organic matter. However, there is a huge difference in hydrocarbon potential between humic and saprophytic organic matter. However, in recent years, great discoveries of shale oil, shale gas, dense sandstone gas and coal bed methane have been made in the exploration of the Dalong Formation of the Upper Permian in Northeastern Sichuan, which also confirms that the Permian shale in Northeastern Sichuan has the potential to produce hydrocarbons, which laterally reflects that the organic matter is the humus type. The abundance of putrescible amorphous bodies suggests that the Late Permian Orogeny mainly received organic matter inputs from planktonic algae and lower microorganisms in the water column, and that the algal bodies were basically degraded to putrescible amorphous bodies by bacteriolysis during the early stages of sedimentary diagenesis [60–63].

Sample X-1 is a core sample of shale from the Dallon Formation at a depth of 4213.35 m, photographed under reflected light from a 5× lens, with large pieces of faunal debris visible in the sample (Figure 2a). Samples X-4 are core samples of shale from the Dalong Formation at a depth of 4229.1 m, photographed under reflected light from a 10× lens, with foraminifera and some faunal debris visible in the samples (Figure 2b). Sample X-13 is a core sample of shale from the Dallon Formation at a depth of 4266.23 m, photographed under reflected light from a 50× oil lens, with solid bitumen and large amounts of pyrite visible (Figure 2c). Sample X-15 is a core sample of shale from the Dallon Formation at a depth of 4270.39 m, photographed under reflected light from a 50× mirror oil lens, which shows a lot of pyrite and a lot of organic matter (Figure 2d).

Samples X-19 are core samples of shale from the Wujiaping Formation at a depth of 4297.28 m. Photographs under reflected light from a 50× oil lens show a large amount of organic matter, mainly solid asphalt specks and filaments as well as many granular pyrites (Figure 3a). Sample X-22 is a core sample of shale from the Wujiaping Formation at a depth of 4310.39 m, photographed under reflected light from a 50× oil lens, rich in organic matter, mainly solid asphalt, with a small amount of specularia, and a large amount of pyrite is visible (Figure 3b). Samples X-20 are core samples of shale from the Wujiaping Formation at a depth of 4297.28 m. Photographs under reflected light from a 50× oil lens are rich in organic matter, with predominantly mirrored bodies and solid asphalt, as well as a small amount of filamentous bodies (Figure 3c). Sample Y-7 is a core sample of shale from the Wujiaping Formation at 3324.38 m, photographed under reflected light from a 50× oil lens, with high organic matter content and large amounts of solid bitumen visible (Figure 3d).

Sample Y-14 is a core sample of shale from the Maokou Formation at a depth of 3355.47 m. Photographs under reflected light from a 50× oil lens show a large block of solid bitumen (with many holes on the surface), trace amounts of pyrite, and a small amount of filamentous bodies (Figure 4a). Samples Y-14 show reflected light characteristics, visible solid bitumen, very high organic matter content, at overmature stage, non-fluorescent (Figure 4b). Sample Y-10 is a core sample of shale from the Maokou Formation at a depth of 3340.54 m. Photographs under reflected light from a 10× lens show a large amount of faunal debris, mainly dominated by radiolarians (Figure 4c). Sample Y-7 is a core sample of shale from the Maokou Formation at a depth of 3324.38 m, photographed under transmitted light from a 50× oil lens; the organic matter content is so high that the light does not penetrate through the light sheet, and many radiolarians can be seen (Figure 4d).

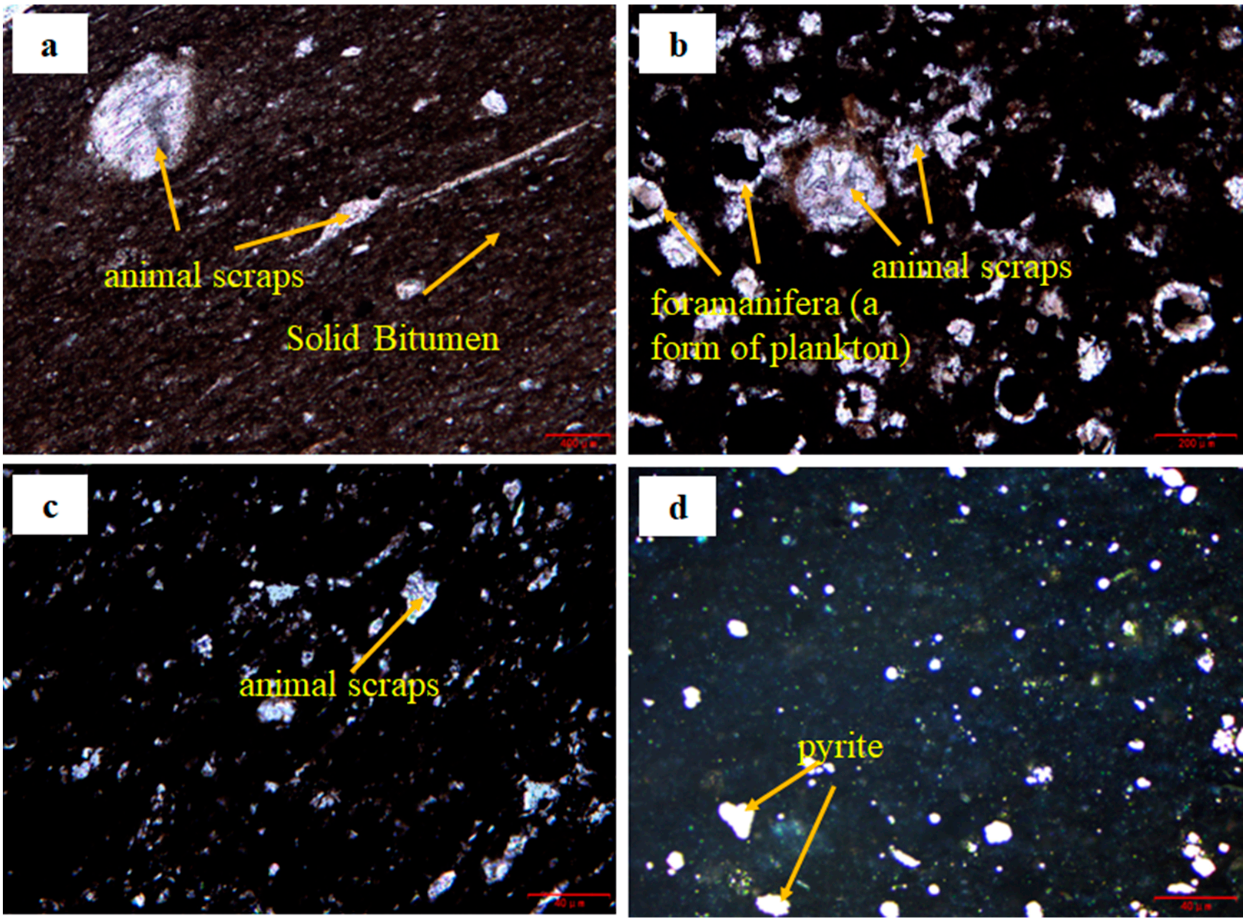

Figure 2. Photomicrographs of light thin section samples from the Permian Dalong Formation, northeast Sichuan, China. (**a**) is sample X-1, (**b**) is sample X-4, (**c**) is sample X-13, and (**d**) is sample X-15.

4.2. Trace Element Characteristics and Palaeoenvironmental Significance

Changes in the depositional environment may lead to anomalous enrichment or severe deficit of some trace elements during deposition, and therefore, changes in some trace elements can be used to indicate the depositional environment. According to the specific geological and tectonic background of northeastern Sichuan, the factors related to the genesis and enrichment of organic matter mainly include regional geology and tectonics, hydrothermal activity, palaeoredox environments, palaeoclimatic changes, and palaeosalinity. (Figure 5) Therefore, this study analyses the elemental geochemical characteristics of shales from the Permian Dalong Formation, Wujiaping Formation and Maokou Formation in northeast Sichuan and explores the palaeobathymetry, palaeoproductivity, palaeoredox environment, palaeoclimate, and palaeosalinity during the stratigraphic depositional period of their strata through the trace element characteristics [60–63]. Some trace element data of the Permian shale in northeast Sichuan are shown in Table 3 and Figure 5.

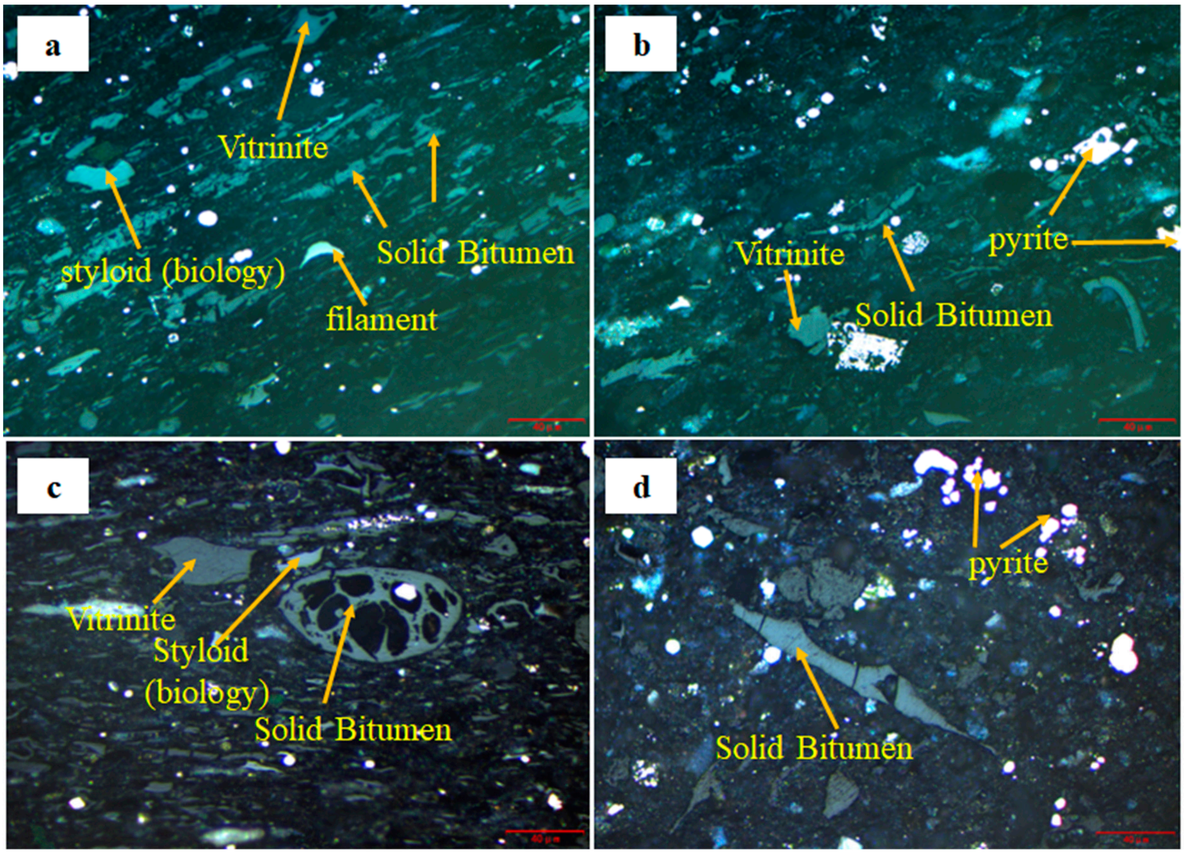

Figure 3. Photomicrographs of light thin section samples of the Permian Wujiaping Formation, northeast Sichuan, China. (**a**) is sample X-19, (**b**) is also sample X-22, (**c**) is sample X-20, and (**d**) is sample Y-7.

4.3. Organic Matter Maturity

Mud shale organic matter maturity is an important indicator for evaluating the degree of thermal derivatisation of organic matter in hydrocarbon source rocks, and the most commonly used is the specular body reflectance, Ro. In this study, whole-rock specular plasma reflectance was determined for 18 of 40 samples from Permian shales in northeastern Sichuan (Tables 4 and 5). Microscopic observation shows that the abundance of vitrinite in the Permian shale samples in northeast Sichuan is generally low. The vitrinite is mainly unstructured vitrinite and detrital vitrinite, and the vitrinite is generally distributed in small granular and band-like layers. Only a very small number of samples can be found to meet the test standards [63].

Table 3. Statistics of some trace element ratios of Permian shale in northeast Sichuan Province.

Stratum	Number of Samples/pc	La/Ce	Sc/Cr	Y/Ho	Sr/Cu	Sr/Ba	U/Th	Mo/U
Dalong Formation	15	0.38~0.81 /0.57	0.01~0.16 /0.07	23.33~38.64 /30.57	0.08~4.17 /1.13	0.53~34.36 /6.53	0.36~63.64 /9.03	0.06~15.68 /5.31
Maokou Formation	10	1.06~1.51 /1.21	0~0.18 /0.04	26.02~46.45 /34.35	0.02~1.69 /0.71	0.57~48.81 /22.09	11.65~24.20 /17.89	1.26~7.64 /4.47
Wujiaping Formation	15	0.42~0.54 /0.48	0.01~0.25 /0.12	23.75~47.51 /31.36	0.06~1.88 /0.53	0.35~7.56 /2.55	0.17~4.84 /1.34	0.41~17.47 /4.11

Remarks: Minimum~Maximum/Average values.

Table 4. Whole-rock reflectivity of Permian X-well shale in northeastern Sichuan Province.

Sample Number	Sampling Depth/m	Stratum	Whole Rock Reflectance/%			
			Minimum Value	Maximum Values	Average Value	Measured Point
X-2	4216.25	Dalong Formation	0.93	1.45	1.14	22
X-4	4229.1		1.33	1.84	1.52	32
X-6	4243.1		1.38	1.96	1.66	25
X-8	4247.13		1.76	2.28	1.98	24
X-10	4253.69		1.9	2.44	2.2	22
X-12	4263.09		2.02	2.69	2.42	42
X-14	4268.47		1.8	2.29	2.07	25
X-17	4280.78	Wujiaping Formation	2.14	2.68	2.57	18
X-20	4297.28		1.61	2.47	2.01	22
X-22	4310.39		1.83	2.27	2	22
X-24	4330.48	Maokou Formation	1.99	2.5	2.25	35
X-26	4333.75		1.25	1.94	1.46	44

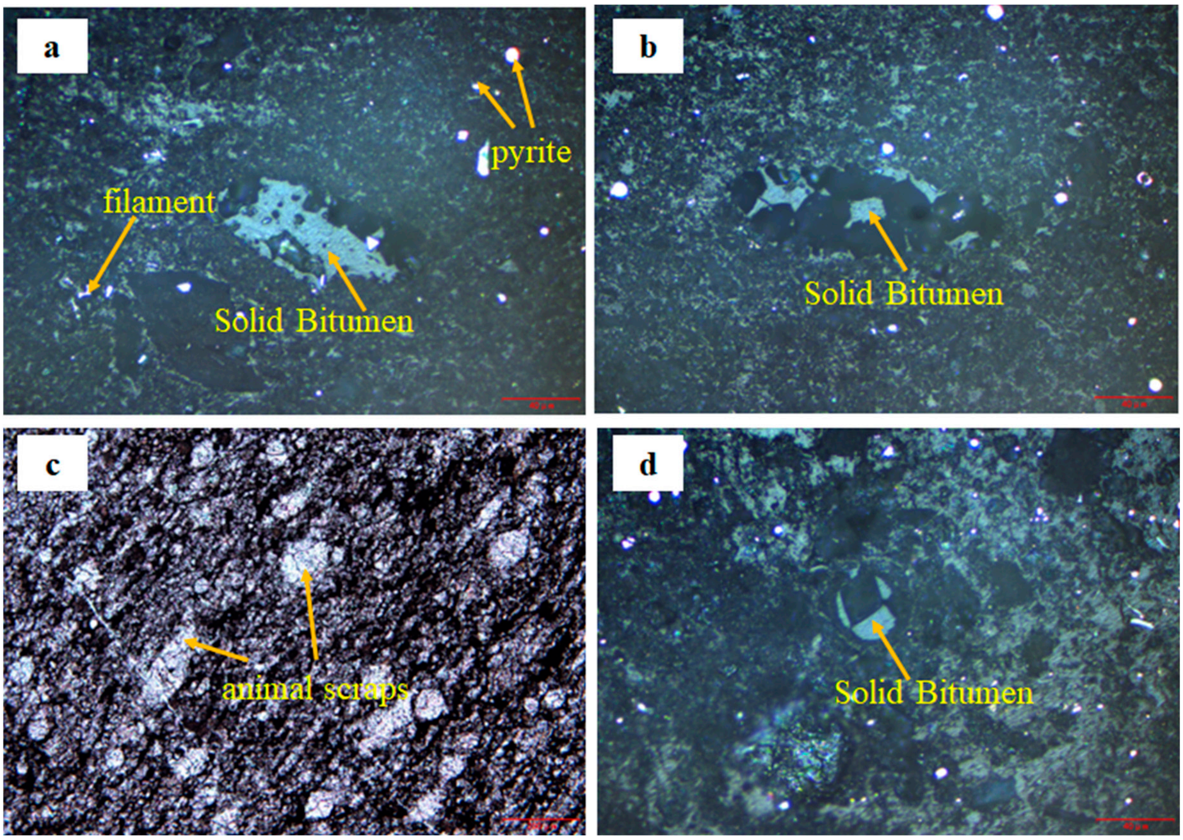

Figure 4. Photomicrographs of light thin section samples from the Permian Maokou Formation, northeast Sichuan, China. (**a**) is sample Y-14, (**b**) is also sample Y-14, (**c**) is sample Y-10, and (**d**) is sample Y-7.

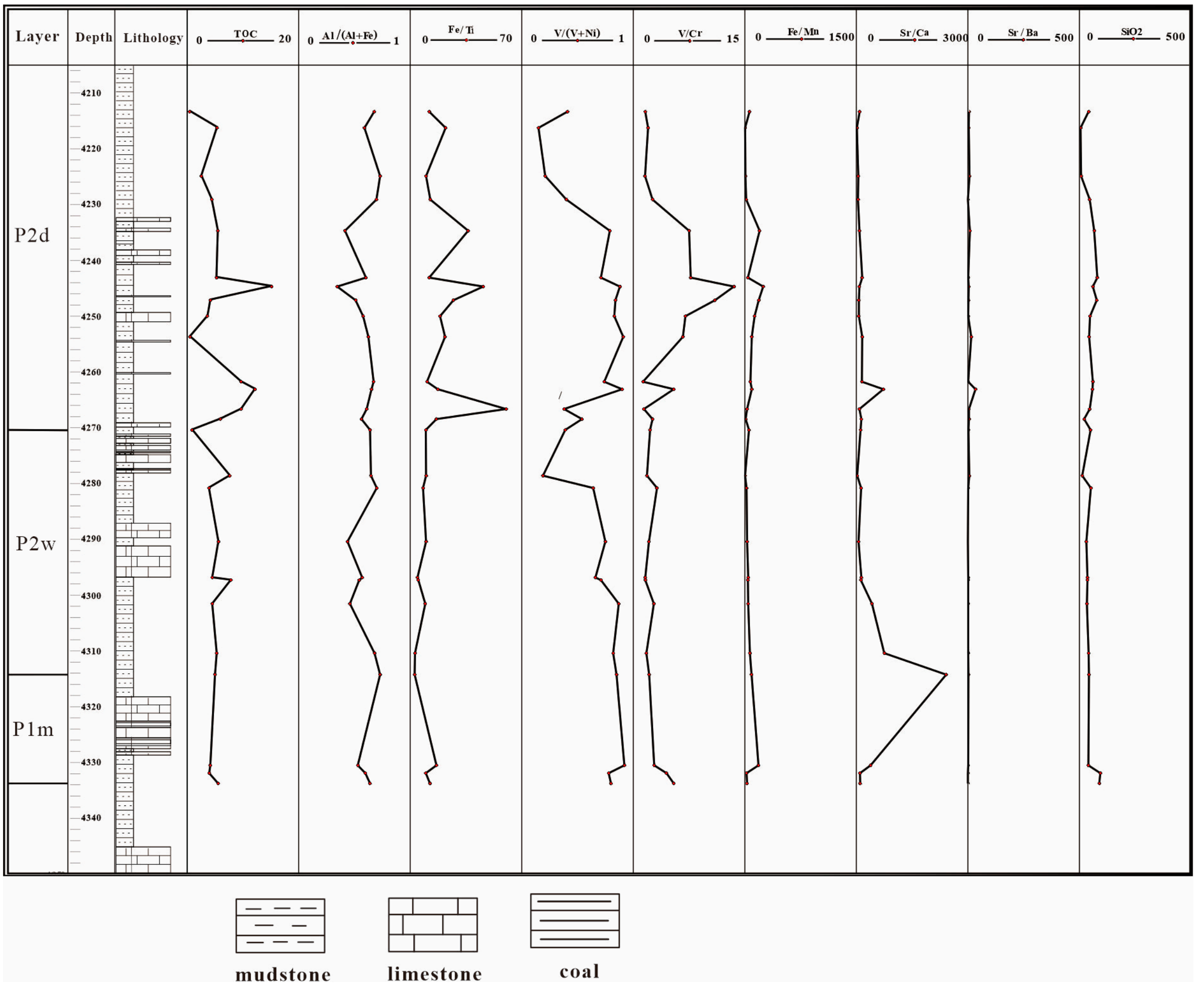

Figure 5. Trace element relationships for X wells in the Permian of northeastern Sichuan Province.

Table 5. Whole-rock reflectivity of Permian L-well shale in northeastern Sichuan Province.

Sample Number	Sampling Depth/m	Stratum	Whole Rock Reflectance/%			
			Minimum Value	Maximum Values	Average Value	Measured Point
Y-3	3304	Wujiaping Formation	1.91	2.32	2.13	50
Y-5	3308.7		2.04	2.59	2.32	43
Y-6	3323.38		1.61	2.09	1.82	58
Y-8	3333.54	Maokou Formation	1.67	2.26	1.94	25
Y-11	3345.07		2.07	2.66	2.47	68
Y-14	3355.47		1.8	2.43	2.03	38

The experimental results show that the whole-rock reflectivity of the Northeast Sichuan Permian is generally high, with the lowest value being 0.93, the highest value being 2.69, and the average value being 1.86 in the Dalong Formation, which belongs to the stage of high-mature cracked gas; the whole-rock reflectance of the Wujiaping Formation ranges from 1.25 to 2.68, with an average value of 2.14, which belongs to the overmature stage. The whole-rock reflectance of the Maokou Formation ranges from 1.25 to 2.66, with an average value of 2.03 belonging to the overmature stage. Therefore, the whole-rock albedo of the Permian shales in northeast Sichuan is generally high, with a high degree of thermal evolution, belonging to the overmature stage, and showing no fluorescence under the microscope [63].

Raman spectra can reflect the information of atomic and molecular vibrations in the aromatic carbon ring structure of organic matter, i.e., the parameters of the Raman spectral peaks of organic matter respond well to the changes in the chemical structure of organic matter during thermal evolution, and thus characterise the maturity. The peak spacing between the D and G peaks has been shown to be the most reliable indicator of maturity. The G (1580–1600 cm^{-1}) and D (1350–1380 cm^{-1}) peaks correspond to the E2g stretching vibrational modes of the graphite aromatic layer and the defects of the aromatic lattice, respectively. The current study used Equation [63]:

$$Ro_{Rmc} = 0.0537d(G - D) - 11.21 \quad (1)$$

The reflectance converted from Raman spectral peaks and the above equation in the current study basically matches the local organic matter maturity characteristics, but it is generally higher than the measured values, which is in line with the previous studies. (Table 6) This converted value is larger than the measured value mainly because the Permian shales in Northeast Sichuan are generally in the high-overmature stage, and most of the organic matter is decomposed into fine particles under thermal maturation, making it difficult to distinguish the lenticular group, the inertial group, and the crustal group under the microscope. Especially for dispersed sedimentary organic matter (mudstone, shale, etc.), the fine vitrinite fragments and the relatively high content of transition components such as hemimirror and hemifilament in lacustrine sedimentary environments make it difficult to accurately distinguish each microscopic component [64]. Therefore, the problem of identification of microscopic components in the present study may be the main reason for the higher calculated reflectance values of Raman parameters than the measured reflectance values of specular bodies.

Table 6. Partial Raman spectral parameters and specular body reflectance of Permian shale in Northeast Sichuan Province.

Sample Number	Mt Raman	Raman Shift/cm	d(G − D)/cm	Ro_{Rmc}/%	$Ro_{reality}$/%
X-20-1	D G	1347.4 1598	250.6	2.25	2.01
X-20-3	D G	1334.7 1599.5	264.8	3	
X-22-1	D G	1339.4 1598	258.6	2.67	2
X-22-3	D G	1336.7 1598	261.3	2.8	
Y-14-2	D G	1342.2 1599.5	257.5	2.62	2.03
Y-5-3	D G	1342.3 1599.5	257.2	2.6	2.32

5. Discussion

5.1. Palaeodepositional Environments

5.1.1. Palaeobathymetric Characteristics

The migration and enrichment patterns of both Rb and K elements in water are closely related to those of clay, but Rb is more easily transported by adsorption on clay compared to K. Therefore, Rb/K values are often used to indicate changes in water depth, with larger values revealing a deeper body of water. Zr is a land-friendly element, and the farther away from the terrestrial source area, the lower the elemental content. The distribution of Zr in sedimentary rocks is dominated by the element Al, so Zr/Al values can represent changes in the land-source component of proximity transport and the depth of the water column, with smaller values indicating greater distance offshore and deeper water bodies. In the intersection map (Figure 6a), shale samples from the Dalong Formation are mainly concentrated in the lower right area, indicating that the Dalong Formation has larger Rb/K values and relatively smaller Zr/Al values, which suggests that the palaeohydrological body of the Dalong Formation is deeper compared to the Wujiaping and Maokou Formations. Meanwhile, the Zr/Al values of the Wujiaping Formation are larger and the Rb/K values are smaller, indicating that the palaeohydrology of the Wujiaping Formation is shallower. Comprehensive analysis shows that the depth of the Dalong Formation is the deepest, followed by the Maokou Formation, and the shallowest is the Wujiaping Formation; the analysis also indicates that the depositional periods of the Dalong and Maokou Formations were farther offshore, and the Wujiaping Formation was closer offshore.

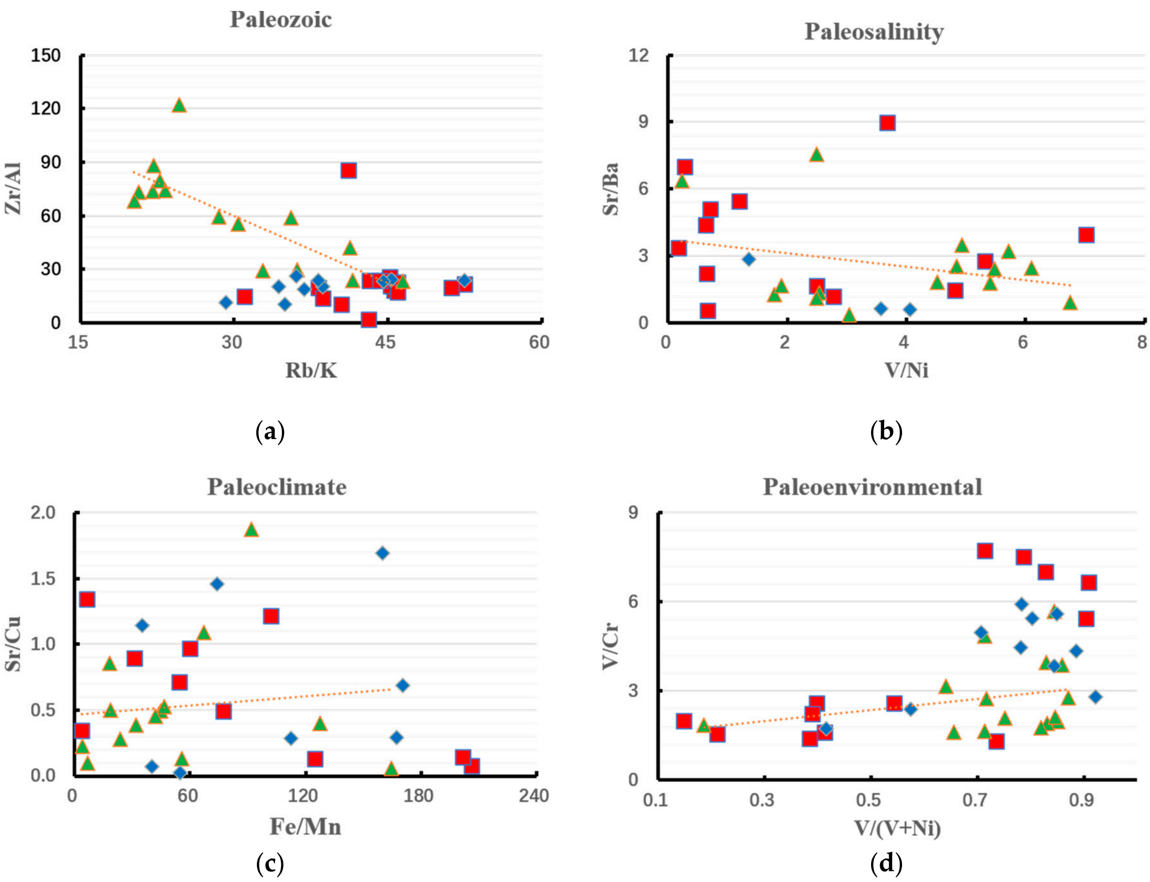

Figure 6. Intersection of palaeoenvironmental indicators of the Dalong, Wujiaping and Maokou Formations. Red represents the Dalong Formation, green represents the Wujiaping Formation, and blue represents the Maokou Formation. (**a**) paleozoic; (**b**) paleosalinity; (**c**) paleoclimate; (**d**) paleoenvironmental

5.1.2. Palaeosalinity Characteristics

Because Sr has a stronger migration capacity than Ba and Ca, in seawater Ba^{2+} and Ca^{2+} will be attracted to SO_4^{2-} in seawater and precipitate as barium sulphate and calcium sulphate. When the salinity of seawater does not reach a certain high value, Sr will continue to migrate with the seawater to the far sea, until the seawater salinity is high enough to produce strontium sulphate precipitation. Therefore, we can use Sr/Ba or Sr/Ca as an indicator of the salinity of seawater, and the larger the ratio, the saltier the seawater. Values of Sr/Ba less than 0.6 are generally regarded as freshwater, 0.6 to 1.0 as brackish, and greater than 1.0 as saline. From Figure 6b, it can be seen that the Dalong Formation, Wujiaping Formation and Maokou Formation are all brackish water environments. The solubility of

V and Ni elements varies when the salinity of the water body is different, and the higher V/Ni value reflects the higher salinity of the water body [65].

The solubility of the elements V and Ni varies when the salinity of the water body is different; the higher the V/Ni value, the higher is the salinity of the water body. Figure 6b reveals that the Dalong Formation is in the lower left corner of the intersection map, while the Wujiaping Formation is in the lower right corner of the intersection map; this suggests that the Wujiaping Formation, the Maokou Formation and the Dalong Formation are all in brackish environments. The V/Ni values are higher in the Wujiaping Formation and lower in the Dalong Formation; the palaeohydrates of the Wujiaping Formation are more saline, the Dalong Formation is lower, and the Maokou Formation is located between the two [66,67].

5.1.3. Palaeoclimatic Characteristics

The values of Sr/Cu are very sensitive to palaeoclimate changes and can therefore be used as an indicative parameter of palaeoclimate changes during the depositional period; the element Sr prefers dryness and the element Cu prefers wetness. Sr/Cu values less than 5 indicate a humid climate; values between 5 and 10 indicate a semi-humid climate, and values greater than 10 indicate an arid climate.

Fe/Mn values can also be used as an indicator of palaeoclimate, with high values indicating humid climates and low values indicating arid climates. Of these, Fe tends to accumulate rapidly in humid environments, while Mn is very low in humid environments and high in arid environments. From Figures 5 and 6, we can see that the Northeast Sichuan Permian is basically in an anoxically reduced still-sea environment, corroborating the results of the intersection diagram.

In the present study, the Sr/Cu values of the Dalong Formation ranged from 0.08 to 1.22, with an average value of 0.64, indicating that its depositional environment was a humid climate. In contrast, the value of Fe/Mn ranged from 3.69 to 206 with a mean value of 90.26, indicating its arid climate. In general, the values reflect the semi-humid climatic conditions of the Dallon Formation. The Sr/Cu values of the Wujiaping Formation range from 0.06 to 0.85, with an average value of 0.39, indicating that Sr/Cu deposition occurred in a humid climate. The value of Fe/Mn ranges from 4.0 to 164, with an average value of 49.14, reflecting that the Wujiaping Formation was formed under semi-humid-arid climatic conditions in general. In the palaeoclimate index convergence diagram (Figure 6c), the sample points of the Wujiaping Formation are relatively concentrated in the upper left, reflecting the arid climate in this depositional period. The Dallon Formation sample site is divided into two parts, reflecting changes in the climatic environment that occurred during the depositional period of the Dallon Formation. Combined with the longitudinal map, the analysis suggests that the palaeoclimatic environment of the Dalong Formation changed from an arid climate to a semi-humid climate [67–69].

5.1.4. Paleoredox Characterization

It is generally accepted that trace elements such as V, Ni, Cd, Sc, Cr, Th, and U are sensitive to the redox properties of the environment and that the elemental abundances and ratios can be used as indicative parameters of redox conditions. However, trace elements in sediments are strongly influenced by inputs from land-based sources of detritus. Therefore, the trace elements in this study must be autochthonous in the oceans, and therefore the influence of terrestrial sources of detrital material must also be considered when discussing the recovery of paleoredox environments by trace elements. Al in shale is mainly derived from clay minerals formed by weathering of terrestrial source clastic materials, so the element Al serves as a signature element indicative of terrestrial source clastic materials. In this next experiment, it was found that the element Al has a strong correlation with U and Th, suggesting that the U and Th in the samples mainly originate from the contribution of terrestrial source detrital material. While V, Ni, Cd, and Cr have no significant correlation with Al, the elements V, Ni, and Cr were adopted as indicative parameters of the palaeoredox environment. A V/Cr value of less than 2 is an oxidising environment, between 2.00 and 4.25 is a moderately reducing environment, and a V/Cr ratio greater than 4.25 is a strongly reducing environment. The V/(V + Ni) value is also an effective indicator of redox conditions, with a ratio of less than 0.46 for an oxidising environment, between 0.46 and 0.57 for a weakly oxidising environment, between 0.57 and 0.83 for an anoxic environment, and between 0.83 and 1.00 for an extremely anoxic environment [60–64].

The trace element results in Figure 6d indicate that the Dalong Formation is a weakly oxidised environment, the Wujiaping Formation is an anoxic environment, and the Maokou Formation is an anoxic environment. This corresponds to the low TOC values of the Dalong Formation compared to those of the Wujiaping and Maokou Formations.

5.2. Types and Characteristics of Organic Microcomponents

The content of saprolite in the shale in the study area is the majority, which mainly exists in the form of saprolite amorphous bodies. Derived from organic matter input from planktonic algae and lower microorganisms in the water column, microcomponents of algae are formed by bacteriolysis during the early stages of sedimentary diagenesis. The biological structures within the algal material will gradually disappear as a result of diagenesis and become clumps with only algal outlines, which may be further degraded and fragmented into clasts that are transformed into diagenetic formations by diagenesis. The humus group is extremely hydrocarbon-generating, and during the thermal maturation stage, the humus group forms a large amount of hydrocarbons. The Permian shales of northeastern Sichuan are in an overall stage of high-overmature thermal evolution. Algal plastids with biological structures have become difficult to observe, and most algae have been thermally degraded to unstructured and microscopic components with no fixed morphology, known as structureless putrescences [67–69].

What follow are secondary components, mainly solid asphaltenes. After the sedimentary organic matter is buried, the disproportionation reaction occurs under the action of factors such as ground temperature, pressure or tectonic stress, generating a new microcomponent that is completely different from the primary microcomponent in terms of structure, morphology and yield and that is called the secondary group. Solid asphalt has no fixed morphological characteristics; its morphology depends entirely on the shape of the endowment pore space, so it is often manifested as strips and irregular shapes.

6. Conclusions

The Permian Dalong Formation, Wujiaping Formation and Maokou Formation in northeast Sichuan are a set of organic hydrocarbon source rocks. The overall TOC is high, with average values of 5.68%, 8.8% and 7.89%, respectively, and is generally in the high-overmature stage ($1.8 < Ro < 2.6$), which provides a theoretical basis for later shale gas exploration and development.

The microscopic composition of the Permian shale in northeast Sichuan is mainly dominated by the rotting mud group, followed by the inertia group and solid asphalt. Organic matter is mainly derived from organic matter input from planktonic algae and lower microorganisms. Algae are subjected to bacteriolysis in the early stages of sedimentary diagenesis to form a large number of humic fractions, called humic amorphous bodies. During the thermal maturation stage, large amounts of hydrocarbons are formed in the humic group.

The Permian marine hydrocarbon source rocks in the study area were deposited in a continental margin environment, where hydrothermal activity rose along the continental margin, and the dry and hot climatic environment resulted in the formation of sedimentary water bodies far from land-sourced debris. An anaerobic–anoxic non-sulphide hydrostatic sea developed in the early and Late Permian, with anaerobic sulphide hydrostatic environments predominating in the Middle and Late Permian. These factors have contributed to the high quality of the Permian hydrocarbon source rocks and their spatial distribution pattern in northeast Sichuan.

Author Contributions: Conceptualization, C.J. and X.X.; methodology, X.X. and C.J.; data curation, C.J. All authors have read and agreed to the published version of the manuscript.

Funding: Supported by the National Natural Science Foundation of China (41972163, 42173055) and the Outstanding Young Innovative Team Project of the Provincial Department of Education (Hydrocarbon Rock Geochemistry, T2022008).

Institutional Review Board Statement: Not applicable.

Informed Consent Statement: Not applicable.

Data Availability Statement: All data and materials are available upon request from the corresponding author. The data are not publicly available due to ongoing research using a part of the data.

Acknowledgments: We would like to thank Wang Pengwei from the Petroleum Exploration and Development Research Institute of China Petroleum and Chemical Corporation for providing core samples and technical support; and Wang Ye from Chang'an University for his valuable comments. Thank you to the reviewers for their valuable comments.

Conflicts of Interest: The authors declare no conflicts of interest.

References

1. Jarvie, D.M.; Hill, R.J.; Ruble, T.E.; Pollastro, R.M. Unconventional shale-gas systems: The Mississippian Barnett Shale of northcentral Texas as one model for thermogenic shale-gas assessment. *AAPG Bull.* **2007**, *91*, 475–499. [CrossRef]
2. Loucks, R.G.; Ruppel, S.C. Mississippian Barnett shale: Lithofacies and depositional setting of a deep-water shale-gas succession in the Fort Worth basin, Texas. *AAPG Bull.* **2007**, *91*, 579–601. [CrossRef]
3. Guo, X.S.; Hu, D.F.; Li, Y.P.; Liu, R.B.; Wang, Q.B. Geological features and reservoiring mode of shale gas reservoirs in Longmaxi Formation of the Jiaoshiba area. *Acta Geol. Sin.-Engl. Ed.* **2014**, *88*, 1811–1821. [CrossRef]
4. Jin, Z.J.; Hu, Z.Q.; Gao, B.; Zhao, J.H. Controlling factors on the enrichment and high productivity of shale gas in the Wufeng Longmaxi Formation, southeastern Sichuan Basin. *Earth Sci. Front.* **2016**, *23*, 1–10.
5. Liu, H.L.; Wang, H.Y.; Fang, C.H. The formation mechanism of over-pressure reservoir and target screening index of the marine shale in the South China. *Earth Sci. Front.* **2016**, *23*, 48–54.
6. Nie, H.K.; Li, D.H.; Liu, G.X.; Lu, Z.Y.; Wang, H.; Wang, R.Y.; Zhang, G.R. An overview of the geology and production of the Fuling shale gas field, Sichuan Basin, China. *Energy Geosci.* **2020**, *1*, 147–164. [CrossRef]
7. Tan, J.; Horsfield, B.; Fink, R. Shale gas potential of the major marine shale formations in the upper Yangtze platform, south China, Part III: Mineralogical, Lithofacial, petrophysical, and rock mechanical properties. *Energy Fuels* **2014**, *28*, 2322–2342. [CrossRef]
8. Zhang, K.; Song, Y.; Jiang, S.; Jiang, Z.; Jia, C.; Huang, Y.; Wen, M.; Liu, W.; Xie, X.; Liu, T. Mechanism analysis of organic matter enrichment in different sedimentary backgrounds: A case study of the Lower Cambrian and the Upper Ordovician-Lower Silurian, in Yangtze region. *Mar. Pet. Geol.* **2018**, *99*, 488–497. [CrossRef]
9. Cao, T.T.; Song, Z.G.; Wang, S.B.; Cao, X.X.; Li, Y.; Xia, J. Characterizing the pore structure in the silurian and permian shales of the Sichuan Basin, China. *Mar. Petrol. Geol.* **2015**, *61*, 140–150. [CrossRef]
10. Cao, T.T.; Xu, H.; Liu, G.X.; Meng, M.; Cao, Q.G.; Yu, Y. Factors influencing microstructure and porosity in shales of the WufengLongmaxi formations in northwestern Guizhou, China. *J. Pet. Sci. Eng.* **2020**, *181*, 107181. [CrossRef]
11. Nie, H.; Zhang, J.; Jiang, S. Types and characteristics of the lower silurian shale gas reservoirs in and around the Sichuan basin. *Acta Geol. Sin.-Engl. Ed.* **2017**, *89*, 1973–1985.
12. Tian, H.; Pan, L.; Xiao, X.; Wilkins, R.; Meng, Z.; Huang, B. A preliminary study on the pore characterization of Lower Silurian black shales in the Chuandong Thrust Fold Belt, southwestern China using low pressure N2 adsorption and FE-SEM methods. *Mar. Pet. Geol.* **2013**, *48*, 8–19. [CrossRef]
13. Wang, C.; Zhang, B.; Lu, Y.; Shu, Z.; Lu, Y.; Bao, H.; Meng, Z.; Chen, L. Lithofacies distribution characteristics and its controlling factors of shale in Wufeng Formation-Member 1 of Longmaxi Formation in the Jiaoshiba Area. *Pet. Res.* **2018**, *3*, 306–319. [CrossRef]
14. Wang, Y.; Liu, L.; Zheng, S.; Luo, Z.; Sheng, Y.; Wang, X. Full-scale pore structure and its controlling factors of the WufengLongmaxi shale, southern Sichuan Basin, China: Implications for pore evolution of highly overmature marine shale. *J. Nat. Gas Sci. Eng.* **2019**, *67*, 134–146. [CrossRef]
15. Xu, Z.; Shi, W.; Zhai, G. A rock physics model for characterizing the total porosity and velocity of shale: A case study in Fuling area, China. *Mar. Pet. Geol.* **2019**, *99*, 208–226. [CrossRef]
16. Yang, F.; Ning, Z.F.; Wang, Q.; Zhang, R.; Krooss, B.M. Pore structure characteristics of lower Silurian shales in the southern Sichuan Basin, China: Insights to pore development and gas storage mechanism. *Int. J. Coal Geol.* **2016**, *156*, 12–24. [CrossRef]

17. Milliken, K.L.; Rudnicki, M.; Awwiller, D.N.; Zhang, T. Organic matter-hosted pore system, Marcellus formation (Devonian), Pennsylvania. *AAPG (Am. Assoc. Pet. Geol.) Bull.* **2013**, *97*, 177–200. [CrossRef]
18. Peng, N.; He, S.; Hu, Q.H.; Zhang, B.Q.; He, X.P.; Zhai, G.Y.; He, C.C.; Yang, R. Organic nanopore structure and fractal characteristics of Wufeng and lower member of Longmaxi shales in southeastern Sichuan, China. *Mar. Pet. Geol.* **2019**, *103*, 456–472. [CrossRef]
19. Wu, L.Y.; Hu, D.F.; Lu, Y.C.; Liu, R.B.; Liu, X.F. Advantageous shale lithofacies of Wufeng Formation-Longmaxi Formation in Fuling gas field of Sichuan Basin, SW China. *Pet. Explor. Dev.* **2016**, *43*, 189–198, (In Chinese with English Abstract). [CrossRef]
20. Zou, C.; Dong, D.; Li, J.Z.; Wang, S.J.; Li, X.J.; Wang, Y.M.; Li, D.H.; Huang, J.L. Shale gas resource potential and prospect of exploration and development. *Geol. Bull.* **2011**, *30*, 324–336.
21. Wang, Z. Practice and cognition of shale gas horizontal well fracturing stimulation in Jiaoshiba of Fuling area. *Oil Gas Geol.* **2014**, *35*, 425–430.
22. Wang, S. *The Tectonic Characteristics of Changning Area, South of Sichuan and Crack Characteristics of Longmaxi Formation of Silurian System*; Chengdu University of Technology: Chengdu, China, 2014.
23. Zhou, D. *Shale Gas Reservoiring Conditions and Favorable Area Preferred in Lower Paleozoic in Sichuan Weiyuan Area*; Chengdu University of Technology: Chengdu, China, 2013.
24. Guo, T.; Zhang, H. Formation and enrichment mode of Jiaoshiba shale gas field, Sichuan Basin. *Pet. Explor. Dev.* **2014**, *41*, 28–36. [CrossRef]
25. Liu, Z.B.; Li, P.; Liu, G.X.; Li, X.; Liu, H.T.; Wang, P.W.; Hao, J.Y.; Li, Q.W. Organic geochemical characterization of the Lower Permian shale in the northeastern Sichuan Basin, China: Implication for shale gas exploration potential. *Mar. Pet. Geol.* **2019**, *106*, 161–172.
26. Guo, Z.H.; Hu, G.Y.; He, K.; Mi, J.K.; Tian, L.J.; He, F.; Guo, C.Y.; Lu, M.D. Geochemical characteristics and depositional environments of hydrocarbon source rocks of the Permian Dalong Formation in northern Sichuan. *Rocky Reserv.* **2023**, *35*, 139–152.
27. Lian, M.L.; Liu, D.D.; Lin, R.Q.; Wang, Y.S.; Shi, F.L.; Cai, J.Y.; Fan, Q.Q.; Zhang, Z.Y.; Zhao, F.P.; Chen, Y.; et al. Depositional environments and organic matter enrichment mechanism of Wufeng Formation-Longmaxi Formation shales in northern Guizhou. *J. Cent. South Univ. (Nat. Sci. Ed.)* **2022**, *53*, 3756–3772.
28. Xie, Z.Y.; Yang, C.L. Geochemical characteristics and genesis of the Middle Devonian and the Middle Permian natural gas in the Sichuan Basin, China. *Nat. Gas Geosci.* **2020**, *5*, 185–198. [CrossRef]
29. Xie, S.; Zhang, J.; Gan, D. Organic geochemical characterization of the Lower Permian black shales in the northeastern Sichuan Basin, South China. *Mar. Pet. Geol.* **2017**, *80*, 165–175.
30. Deng, S.; Tang, X.; Zhang, Y.; Li, L.; Su, B.; Li, X. Organic Geochemical Characteristics and Shale Gas Potential of the Lower Permian Longtan Formation, Northeastern Sichuan Basin, China. *Energy Fuels* **2020**, *34*, 875–888.
31. Cao, Y.; Tang, X.; Zhang, Y.; Luo, P.; Kang, X.; Yue, D. Organic geochemical characteristics and depositional environment of Lower Permian shale in Jiaoshiba area, northeastern Sichuan Basin, China: Implications for shale gas potential. *J. Pet. Sci. Eng.* **2019**, *173*, 722–735.
32. Zhang, Y.; Tang, X.; Hu, P.; Cao, Y.; Deng, S. Organic and inorganic geochemical characteristics of the Lower Permian shale in eastern Sichuan Basin, China: Implications for shale gas potential. *J. Nat. Gas Sci. Eng.* **2018**, *62*, 10–21.
33. Hu, P.; Wang, J.; Zhang, J.; Deng, J.; Jia, C.; Ma, J.; Huang, S. Organic Geochemistry and Depositional Environment of Lower Permian Shale in the Jiaoshiba Area, Northeastern Sichuan Basin, China. *Chin. J. Geochem.* **2017**, *36*, 432–443.
34. Ma, J.; Hu, P.; Zhang, J.; Huang, S.; Jia, C. Organic geochemical properties and source rock potential of the Lower Permian shale in the Jiaoshiba area, northeastern Sichuan Basin, Southwest China. *Arab. J. Geosci.* **2019**, *12*, 340.
35. Zhai, G.M. *Petroleum Geology of China*; Petroleum Industry Press: Beijing, China, 1992. (In Chinese)
36. Li, J.; Xie, Z.Y.; Dai, J.X.; Zhang, S.C.; Zhu, G.Y.; Liu, Z.L. Geochemistry and origin of sour gas accumulations in the northeastern Sichuan Basin, SW China. *Org. Geochem.* **2005**, *36*, 1703–1716. [CrossRef]
37. Huang, J.Q. *On Major Tectonic Units of China*; Geological Press: Beijing, China, 1954; 161p.
38. Wang, Y.Y.; Liu, H.Y.; Wen, Y.C.; Yang, Y.; Zhang, J. Distribution law, exploration method and prospect of the oolitic beach reservoirs in the Feixianguan formation in northeast Sichuan Basin. *Nat. Gas Ind.* **2002**, *22*, 14–18.
39. Wang, B.J. *The Sichuan Hydrocarbon Province*; Volume 10 of Petroleum Geology of China; Petroleum Industry Press: Beijing, China, 1989; p. 516.
40. Ma, Y.S. Petroleum geology of the Puguang sour gas field in the Sichuan Basin, SW China. *Mar. Pet. Geol.* **2008**, *25*, 357–370. [CrossRef]
41. Wang, A.; Xiao, K.H.; Liu, Z.Q.; Huang, Y.Q. Sedimentary facies of the second and third sections of the Yuan Dam in northeastern Sichuan and their effect on reservoir control. *Geoscience* **2023**, 1–16.
42. Liu, S.; Fan, C.; Zhang, B.; Zhang, Y.; Wang, W.; Luo, B.; Bai, X. Characteristics of the Lone Peak Section of the Middle Permian Maokou Formation in the eastern Sichuan Basin and its petroleum geological significance. *Oil Gas Geol.* **2023**, *44*, 993–1008.
43. Jiang, D.; Li, P.; Zou, H. Development characteristics of natural fractures of Jurassic shale in Yuanba area of northeast Sichuan and their influence on shale oil and gas enrichment and preservation. *Geoscience* **2023**, 1–16.
44. Zheng, A.; Meng, Z.; Li, K.; Liu, L.; Liu, Y.; Peng, G.; Yi, Y.; Cai, J. Longitudinal heterogeneity characteristics of Permian Wujiaping Shale reservoirs in Hongxing area of eastern Sichuan and their main factors for development. *Nat. Gas Geosci.* **2023**, *34*, 1500–1514.

45. Guo, J.; Hu, G.; He, K. Geochemical characteristics and sedimentary environment of source rocks of the Permian Dalong Formation in northern Sichuan. *Lithol. Reserv.* **2023**, *35*, 139–152.
46. Heng, L.; Tong, Z.; Qiao, H. The Upper Permian Dallong Formation-Wujiaping Formation in the Wangjiang Depression in the Lower Yangtze Area is rich in organic shale element characteristics and paleoenvironmental significance. *Nat. Gas Explor. Dev.* **2023**, *46*, 74–83.
47. Zhou, Y.; Rui, X.; Fan, B.F. Pore development characteristics of Jurassic continental shale in Sichuan Basin. *J. Xi'an Shiyou Univ. (Nat. Sci. Ed.)* **2023**, *38*, 27–37+80.
48. Liu, S.; Gao, P.; Xiao, X.; Liu, R.; Qin, J. Study on organic petrological characteristics of black shale in Wufeng-Longmaxi Formation in Sichuan Basin. *Geoscience* **2022**, *36*, 1281–1291.
49. Ding, J.; Sun, J.; Zhang, J.; Yang, X.; Shi, G.; Wang, R.; Huang, B.; Li, H. Characteristics of shale biomarker compounds in the Dalong Formation in southern Anhui and their geological significance. *J. Earth Sci.* **2023**, *48*, 235–251.
50. Wang, L.; Zhou, H.; Shang, F.; Zhou, X. Geochemical characteristics of black shale elements and sedimentary paleoenvironment restoration in the Cretaceous Qingshankou Formation in northern Songliao Basin. *Chin. J. Geol.* **2022**, *57*, 156–171.
51. Shu, Z.; Zhou, L.; Li, X.; Liu, H.; Zeng, Y. Geological characteristics and exploration and development prospects of continental shale condensate gas reservoir in the Dongyue Temple section of the Jurassic artesian well formation in the Fuxing area of eastern Sichuan Basin. *Oil Gas Geol.* **2021**, *42*, 212–223.
52. Wang, W.; Shi, W.; Fu, X.; Chen, C. Potential and direction of shale gas exploration in the Dalong Formation of the Permian of northern Sichuan. *Pet. Geol. Exp.* **2020**, *42*, 892–899+956.
53. Liu, Z.; Yuan, B.; Huang, X. Dimigraphic division and comparison of the Permian stratigraphy of Maoertang, Jiange County, northwest Sichuan. *ChengDu Univ. Technol. Acad. J. Cent.* **2020**, *47*, 257–273.
54. Zou, C.; Yang, Z.; Wang, H. "Finding oil from sources": On unconventional continental large-scale shale oil and gas fields in the Sichuan Basin. *Acta Geol. Sin.* **2019**, *93*, 1551–1562.
55. Zhang, K.; Wang, S.; Yang, Y.; Gong, Y.; Zhu, D.; Yang, Y. Development characteristics of dolomite in the Maokou Formation in Puguang area of northeastern Sichuan. *Mar. Orig. Pet. Geol.* **2019**, *24*, 20–26.
56. Zhang, Y.; Xu, S.; Cheng, H.; Lin, L.; Dong, Y.; Yu, Y.; Zhang, Y. Geochemical characteristics of Qixia Formation and its paleoenvironmental significance in Wangcang area of northeastern Sichuan. *Pet. Geol. Exp.* **2018**, *40*, 210–217.
57. *GB/T 19145-2022*; Determination of total Organic Carbon in Sedimentary Rocks. State Administration of Market Supervision and Administration of China and the National Standardization Administration of China: Beijing, China, 2022.
58. *SYT 5124-2012*; Method for Determining the Reflectivity of Specular Bodies in Sedimentary Rocks. National Energy Administration of China: Beijing, China, 2012.
59. *SY/T 6414-2014*; Microcomponent Identification and Statistical Methods for Whole-Rock Light Sheets. National Energy Administration of China: Beijing, China, 2014.
60. Murray, R.W. Chemical Criteria to identify the depositional environment of chert: Deneral principles and applications. *Sediment. Geol.* **1994**, *90*, 213–232. [CrossRef]
61. Borjigin, T.; Lu, L. Formation, preservation and connectivity control of organic pores in shale. *Pet. Explor. Dev.* **2021**, *4*, 84. [CrossRef]
62. Yang, M.; Zuo, Y.; Fu, X.; Qiu, L.; Li, W.; Zhang, J.; Zheng, Z.; Zhang, J. Paleoenvironment of the Lower Ordovician Meitan Formation in the Sichuan Basin and Adjacent Areas, China. *Minerals* **2022**, *12*, 75. [CrossRef]
63. Liu, D.; Xiao, X.; Tian, H.; Tian, H.; Min, Y.; Zhou, Q.; Cheng, P. Methodology and geological application of Raman spectroscopic parameters of solid organic matter to calculate the degree of thermal evolution of samples. *Sci. Bull.* **2013**, *58*, 1228–1241.
64. Wang, Y.; Qiu, N.; Xie, X. Integrated assessment of thermal maturity of the Upper Ordovician–Lower Silurian Wufeng–Longmaxi shale in Sichuan Basin, China. *Mar. Pet. Geol.* **2019**, *100*, 447–465. [CrossRef]
65. Liu, H.; Tong, Z.; Qiao, H.; Wang, S. Elemental characteristics and paleoenvironmental significance of organic-rich shale from the Upper Permian Dalong Formation—Wujiaping Formation, Wangjiang Argumentary Depression, Lower Yangzi Region. *Nat. Gas Explor. Dev.* **2023**, *46*, 74–83.
66. Wang, Y.; Qiu, N.; Xie, X.; Ni, T.; Cheng, H.; Zou, Z.; Ma, Z.; Shen, B.; Borjigin, T. Thermal maturity calibration of extremely high-mature pre-Devonian strata: A case study from the Lower Cambrian Qiongzhusi Formation in the Sichuan Basin, South China. *Geoenergy Sci. Eng.* **2023**, *222*, 211411. [CrossRef]
67. Tenger, B.; Qing, J.; Fu, X.; Yang, Y.; Xie, X. Evaluation of source rocks of the Wujiaping Formation of the Upper Permian in northeastern Sichuan. *J. Palaeogeogr.* **2010**, *12*, 334–345.
68. Li, J.; Zhou, S.; Fu, D.; Li, Y.; Ma, Y.; Yang, Y. Oil-source rock correlation for paleo-oil reservoir in the Puguang gas field, northeast Sichuan Basin, southwest China. *Pet. Sci. Technol.* **2016**, *34*, 578–586. [CrossRef]
69. Chen, H.; Xie, X.; Hu, C. Geochemical characteristics of Late Permian sediments in the Dalong Formation of the Shangsi Section, Northwest Sichuan Basin in South China: Implications for organic carbon-rich siliceous rocks formation. *J. Geochem. Explor.* **2012**, *112*, 35–53. [CrossRef]